NASA/CR-2011-216305

Peak Wind Forecasts for the Launch-Critical Wind Towers on Kennedy Space Center/Cape Canaveral Air Force Station, Phase IV

Winifred Crawford
ENSCO, Inc., Cocoa Beach, Florida
NASA Applied Meteorology Unit, Kennedy Space Center, Florida

September 2011

NASA STI Program ... in Profile

Since its founding, NASA has been dedicated to the advancement of aeronautics and space science. The NASA scientific and technical information (STI) program plays a key part in helping NASA maintain this important role.

The NASA STI program operates under the auspices of the Agency Chief Information Officer. It collects, organizes, provides for archiving, and disseminates NASA's STI. The NASA STI program provides access to the NASA Aeronautics and Space Database and its public interface, the NASA Technical Report Server, thus providing one of the largest collections of aeronautical and space science STI in the world. Results are published in both non-NASA channels and by NASA in the NASA STI Report Series, which includes the following report types:

- TECHNICAL PUBLICATION. Reports of completed research or a major significant phase of research that present the results of NASA Programs and include extensive data or theoretical analysis. Includes compilations of significant scientific and technical data and information deemed to be of continuing reference value. NASA counter-part of peer-reviewed formal professional papers but has less stringent limitations on manuscript length and extent of graphic presentations.

- TECHNICAL MEMORANDUM. Scientific and technical findings that are preliminary or of specialized interest, e.g., quick release reports, working papers, and bibliographies that contain minimal annotation. Does not contain extensive analysis.

- CONTRACTOR REPORT. Scientific and technical findings by NASA-sponsored contractors and grantees.

- CONFERENCE PUBLICATION. Collected papers from scientific and technical conferences, symposia, seminars, or other meetings sponsored or co-sponsored by NASA.

- SPECIAL PUBLICATION. Scientific, technical, or historical information from NASA programs, projects, and missions, often concerned with subjects having substantial public interest.

- TECHNICAL TRANSLATION. English-language translations of foreign scientific and technical material pertinent to NASA's mission.

Specialized services also include organizing and publishing research results, distributing specialized research announcements and feeds, providing help desk and personal search support, and enabling data exchange services.

For more information about the NASA STI program, see the following:

- Access the NASA STI program home page at *http://www.sti.nasa.gov*

- E-mail your question via the Internet to help@sti.nasa.gov

- Fax your question to the NASA STI Help Desk at 443-757-5803

- Phone the NASA STI Help Desk at 443-757-5802

- Write to:
  NASA STI Help Desk
  NASA Center for AeroSpace Information
  7115 Standard Drive
  Hanover, MD 21076-1320

NASA/CR-2011-216305

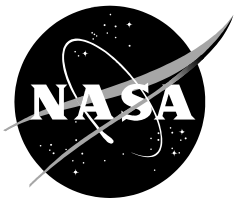

Peak Wind Forecasts for the Launch-Critical Wind Towers on Kennedy Space Center/Cape Canaveral Air Force Station, Phase IV

Winifred Crawford
ENSCO, Inc., Cocoa Beach, Florida
NASA Applied Meteorology Unit, Kennedy Space Center, Florida

National Aeronautics and
Space Administration

Kennedy Space Center
Kennedy Space Center, FL 32899-0001

September 2011

Acknowledgements

The author thanks Mr. William Roeder of the 45th Weather Squadron and Dr. Francis J. Merceret of the Kennedy Space Center Weather Office for lending their statistical expertise to this project, and Mr. Mark Kienzle of ENSCO's GeoSystem Solutions Division for his insight on local stability and for providing data in support of this task.

Available from:

NASA Center for AeroSpace Information
7121 Standard Drive
Hanover, MD 21076-1320
(301) 621-0390

This report is also available in electronic form at

http://science.ksc.nasa.gov/amu/

Executive Summary

The peak winds are an important forecast element for the Expendable Launch Vehicle programs. As defined in the Launch Commit Criteria (LCC), each vehicle has peak wind thresholds that cannot be exceeded in order to ensure safe launch operations. The 45th Weather Squadron (45 WS) launch weather officers (LWOs) indicate that peak winds are challenging to forecast, particularly in the cool season. To alleviate some of the difficulty in making this forecast, the AMU calculated cool season wind climatologies and peak speed probabilities for each of the towers used to evaluate LCC in Phase I (Lambert 2002). In Phase III (Crawford 2010), the AMU updated these statistics with six more years of data, added new time-period stratifications and created a graphical user interface (GUI) to display the values. The 45 WS LWOs and forecasters have seen differences in the tower winds between onshore and offshore flow. Therefore, the 45 WS tasked the AMU to stratify the data by onshore/offshore flow and calculate new climatologies and probabilities to make the statistics more robust and useful to operations.

The data used in this task were from the wind towers in the Kennedy Space Center (KSC)/Cape Canaveral Air Force Station (CCAFS) network used to evaluate weather LCC. The period of record increased from 13 cool seasons (October–April) in Phase III to 16 cool seasons (1995–2010) for this phase. The AMU used automated and manual data quality control methods on the data prior to analysis to ensure erroneous data had a minimal impact on the resulting statistics.

The AMU created climatologies and probabilities of mean and peak wind speeds similar to those in Phase III. The climatologies were hourly means and standard deviations of the 5-min mean and peak speeds during onshore and offshore flow for each month and sensor. Diagnostic onshore and offshore peak speed probabilities were created for each tower in each month for the 5-min mean speeds in 1-kt intervals. "Diagnostic" indicates that the peak speeds were observed in the same 5-min period as mean speed. Empirical, or observed, and parametric distributions fit to the empirical distributions were created. The parametric distribution was calculated to smooth over variations and fill gaps in empirical distributions, and extrapolate probabilities of peak speeds beyond the range of the observations. The Gumbel distribution was used and fit the data well except for some higher speeds.

The next set of statistics to be calculated were the prognostic probabilities that provide the probability of meeting or exceeding a specified peak speed within a specified time period after a 5-min mean speed observation. The time periods requested by the 45 WS were 2, 4, 8, and 12 hours. The AMU used a re-sampling technique developed in Phase III that used all 5-min mean and peak speeds in the data set to calculate the observed probabilities. Due to the extra time needed to modify the algorithm to account for the new $\geq$ 5kt/upwind filters and onshore/offshore stratifications, the AMU was able to complete the 2- and 4-hour probabilities, but not the 8- and 12-hour probabilities.

The AMU modified the GUI developed in Phase III to accommodate the new onshore/offshore stratifications. This GUI was delivered to the 45 WS during development to test and make suggestions for modifications, all of which were incorporated. This ensured that the end product met their needs, was easy to use, and produced useful information in a readable format.

Suggestions for future work include taking into consideration several factors that influence the intensity of peak winds on KSC/CCAFS. These include frontal passages, convective outflow boundaries, and the mixing down of high momentum air from aloft. The atmospheric stability in the boundary layer is also an important factor for gusts, as is the location of the wind sensor relative to the ocean (i.e. how far inland), how much vegetation surrounds the site, and the placement of the sensor relative to the tower.

It is important to remember that all climatology and probability values calculated in this task represent historical wind behavior. They are not predictive, and should not be used as an absolute forecast of future winds. They are intended to assist in making the forecast as an objective first guess. Model output, current observations, and forecaster experience should be used along with this tool to make a confident peak wind forecast.

Table of Contents

List of Figures

List of Tables

1. Introduction

The peak winds are an important forecast element for the Expendable Launch Vehicle programs. As defined in the Weather Launch Commit Criteria (LCC), each vehicle has peak wind thresholds that cannot be exceeded in order to ensure safe launch operations. As a vehicle launches, it could be forced into the tower by a strong wind gust. To avoid this, each launch operation has specific wind speed thresholds defined in the LCC that cannot be exceeded. The thresholds vary by vehicle, vehicle configuration, and wind direction. Launch vehicles are also exposed to the weather from the time their service tower is removed through launch, which could be up to 10 hours. If a launch is scrubbed, the vehicle is exposed for a longer period as it must be de-fueled before its service structure is put back in place. During this time, the vehicle is susceptible to damage from strong winds. Such winds could cause airborne debris to impact and damage the vehicle, or cause the vehicle to oscillate to the point that it damages support lines or makes contact with its supporting structure. Accurate forecasts of peak winds, therefore, are critical to protecting the safety of launch pad workers as well as preventing financial losses due to delays and damage to the vehicle. Such forecasts are valuable to launch directors when deciding not only to launch but whether to continue with pre-launch procedures.

The 45th Weather Squadron (45 WS) indicates that peak winds are a challenging parameter to forecast, particularly in the cool season months October-April. It is also a difficult forecast in the warm season, but the speeds are usually below operational thresholds. If they exceed thresholds, it would likely be due to convection in the area. Other launch and safety criteria would be in effect if convection was close enough to cause high winds. To alleviate some of the difficulty in making the cool season peak wind forecast, the Applied Meteorology Unit (AMU) calculated climatologies and probabilities of 5-min mean and peak winds in Phase I (Lambert 2002). The 45 WS requested the AMU update those statistics in Phase III (Crawford 2010) with more data collected since Phase I was completed, use new time-period stratifications, and test another parametric distribution. They also requested a graphical user interface (GUI) similar to that created in Phase II (Lambert 2003) to display the mean and peak speed climatologies and probabilities. For this phase, the 45 WS tasked the AMU to stratify the data by stability and onshore/offshore flow, and then recalculate the climatologies and probabilities. Stability has long been known to have a strong effect on surface winds, and the 45 WS launch weather officers (LWOs) and forecasters have seen marked differences in the tower winds between onshore and offshore flow. These new stratifications could make the statistics even more robust and useful to operations than the Phase III values.

1.1 Previous AMU Work

In Phase I, the AMU created Microsoft® Excel® (hereafter Excel) PivotCharts that displayed the hourly and directional climatologies for each tower used to evaluate the LCC and the probability of exceeding specific peak speed values given an observed or forecast mean speed value (Lambert 2002). Two classes of probabilities were provided: empirical and parametric. The empirical, or observed, curves for the higher speeds became noisy due to smaller sample sizes. To alleviate this, the AMU fit a parametric distribution to the empirical distributions. This helped smooth the empirical distributions and estimate probabilities of peak speeds outside the range of the observations (Wilks 2006).

The same statistics were calculated in Phase II for the Shuttle Landing Facility (SLF) towers that were used to evaluate the Shuttle Weather Flight Rules (Lambert 2003). The AMU also created a PC-based GUI to display the desired statistical values quickly in a readable format. The PivotChart displays were flexible and allowed the data to be viewed several different ways, but they proved difficult to manipulate and interpret during intensive fast-paced operations. Therefore, the AMU created the GUI using Visual Basic for Applications (VBA) in Excel, which accessed the data in PivotTables.

The goals of Phase III (Crawford 2010) were to update the Phase I statistics for the LCC towers with an increased period of record (POR) from 7 to 13 years, new time-period stratifications, a different parametric distribution, and a GUI similar to the one created in Phase II. The main difference in this work from previous phases was the calculation of prognostic probabilities, i.e. the probability of meeting or exceeding a specified peak speed over the next few hours.

1.2 Current Study

The goals of this task were to update the Phase III statistics for the LCC towers with an increased POR from 13 to 16 years, stratify the data by onshore/offshore flow and stability, and then recalculate the climatologies and probabilities. Due to issues described in this report, the data were not stratified by stability. Section 2 describes the data used in the calculations and how they were stratified and a discussion of the attempt to determine stability. Details of the stability calculations are given in the Appendix. Section 3 describes the calculation of the climatologies and probabilities similar to those in Phase III, and section 4 describes the GUI. A summary is provided in section 5.

2. Data

The wind data used in this task were from the towers in the Kennedy Space Center (KSC)/Cape Canaveral Air Force Station (CCAFS) network used to evaluate LCC. They were provided by Computer Sciences Raytheon. The POR is the cool season months (October–April) in January 1995-December 2010. Data before 1995 were not used due to a known noise problem in the archived peak winds that was fixed in 1994 (William Roeder, 45 WS, personal communication). The stability calculations required the hourly surface pressure observations taken at the SLF. These data were provided by the 14th Weather Squadron.

The wind tower data sets contain the year/month/day/hour/minute/height of each observation with a temporal resolution of 5 minutes. The meteorological variables in the data set included

- Temperature and dew point temperature in Celsius,
- 5-min mean and peak wind speeds in ms^{-1},
- 5-min mean and peak wind direction in degrees,
- Deviation of the 5-min mean wind direction in degrees, and
- Relative humidity in percent.

The raw wind speed and direction were sampled every second. The 5-min mean is the average of 600 1-sec observations in a 5-min period. The peak is the maximum 1-sec speed in the 5-min period. Before processing, the wind speeds were converted to knots (kt) with the conversion factor $kt = 1.9424 * ms^{-1}$. The SLF hourly surface pressure observations were in millibars (mb).

As stated in section 1, the AMU used only cool-season data in the analysis since this was identified by the forecasters as being the most difficult time period in which to forecast peak winds, and it is the period when peak winds approach or exceed the LCC thresholds.

2.1 Wind Towers

The towers and heights used to evaluate the LCC are shown in Table 1. The locations of the pads and towers listed in Table 1 are shown in Figure 1. Data from all towers were available for the entire POR except for those at Space Launch Complex (SLC) 41. The data archive for these towers began in March 2004.

Table 1. Programs, towers, and sensor heights of data that were analyzed in this task.

Launch Program	*Tower(s)*	*Primary Height*	*Backup Height*
Shuttle*	393/394 *(SLC 39A)* 397/398 *(SLC 39B)*	60 ft	N/A
Atlas	41 (primary) 110 (backup)	230 ft 204 ft	N/A 54 ft
Delta II	2	90 ft	54 ft
Delta IV	6 (primary) 108 (backup)	54 ft	12 ft

*Even though the Shuttle Program has ended, data from these towers were included in the analysis for future users of these launch pads.

Figure 1. Map of the KSC/CCAFS area showing the locations of the wind towers described in Table 1.

Towers 2, 6 and 110 have redundant sensors on opposite sides so that one side is always upwind and not affected by the sheltering effect of the tower. Each side has its own number designation as shown in Table 2. The sensors at these towers were added to mitigate the effect of obstructed wind flow around the tower on the downwind sensor. They were also added so that one sensor could be used as a backup in case one failed. The AMU processed and analyzed the data from both sensors at these towers separately. Tower 108 has its sensors mounted on the southeast side only. The towers at SLC 41 and SLC 39A and B are located on the northwest and southeast sides of their respective pads as shown in Figure 1, and each tower has only one sensor.

Table 2. Towers with redundant sensors and the location of the sensors relative to the towers. Each side of the tower is given a distinct number.

Tower Number	*Side: Number*
2	Northwest: 0020 Southeast: 0021
6	Northwest: 0061 Southeast: 0062
110	Northwest: 1101 Southeast: 1102

2.2 Quality Control

The AMU used automated and manual data quality control (QC) methods on the data prior to analysis to ensure erroneous data had a minimal impact on the resulting statistics.

2.2.1 Automated QC

The AMU used the same automated QC algorithms described in Lambert (2002) with the corrections as defined in the Phase II final report (Crawford 2010). The AMU rewrote the QC software in the Java programming language to make it more portable and easier to maintain (Barrett 2010). The Java version uses a configuration text file to contain the algorithm parameters, such as the years in the POR and the list of wind tower identifiers. This allows the user to easily change the parameters by modifying the configuration file. Previously, the user had to edit the source code and recompile the software.

2.2.2 Manual QC

As in Phase III, there were four October days during the POR in which the towers were affected by tropical storm winds: Josephine (1996), Irene (1999), Leslie (2000), and Wilma (2005). The goal of this task is to calculate statistics for cool season winds caused by cool-season phenomena, not tropical storm winds. These data would contaminate the climatology and probability values, so they were manually removed from the subsequent analysis.

2.3 Stratification and Filtering

After QC, the data were stratified by month and sensor (tower/height/side), then by upwind onshore and offshore flow. These data were then filtered to remove records with mean speeds < 5 kt.

2.3.1 Upwind Flow

Use of upwind observations only ensures that the statistics will not be contaminated from using noisy data. Air flow through and around the sides of the tower causes higher standard deviations in speed and direction and less accurate mean and peak wind values in the downwind sensor observations. Tower geometry is important in determining the upwind sector for each sensor.

2.3.1.1 Scaffold Towers

Towers 2, 6, 108 and 110 are square and made with scaffold construction. Air can flow through the scaffolding, but will be disturbed as it does. Figure 2 is a schematic showing the scaffold tower and sensor configuration. The sides of the tower face north (0°), west (270°), south (180°) and east (90°). The northwest sensor is mounted on a boom extending west from and parallel to the north face and the southeast sensor is mounted on a boom extending east from and parallel to the south face. Tower 108 has a sensor on the southeast side only.

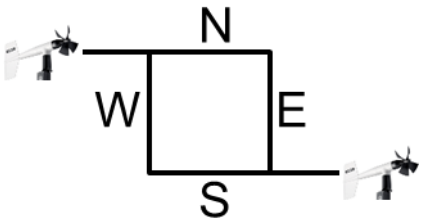

Figure 2. Sensor configuration on the scaffold towers (not to scale).

If upwind is defined solely as flow not through the tower, the sector for the northwest sensor would be 180° through 90° moving clockwise, and 0° through 270° for the southeast sensor. However, flow along the edge of the tower can also be turbulent and cause erroneous wind speeds and directions. Figure 3 shows the sectors used in operations that are considered upwind for the northwest and southeast sensors. The upwind sector is 204° through 68° for the northwest sensor and 23° through 248° for the southeast sensor (Bauman 2010). This provides a buffer of 22°-24° away from the tower sides in order to eliminate this source of turbulence. The resulting wind sectors are 225° wide.

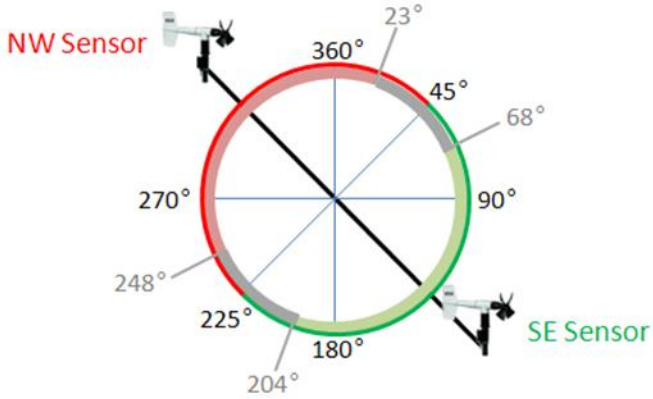

Figure 3. Sensor configuration on Towers 2, 6 and 110. Tower 108 has a southeast sensor only. The northwest sensor is upwind when the winds are between 249° and 22° (light red arc) and the southeast sensor is upwind when the winds are between 69° and 203° (light green arc). The sensor considered upwind in the two gray regions when the winds are 23°-68° or 204°-248° is the one that was upwind before the wind direction changed to those sectors (Bauman 2010 Figure 8).

2.3.1.2 Tower 108

As stated earlier, Tower 108 only has sensors on its southeast side. Therefore, all statistics for this tower were calculated using data from the upwind sector for the southeast sensor, 23°-248°, divided into onshore and offshore flow. There were no statistics calculated for winds from the sector 249°-22° at this tower.

2.3.1.3 SLC 39A and B

The wind sensors at SLC 39A and B are mounted at the top of masts, or solid poles, not on scaffold towers as illustrated in Figure 2. Therefore, the upwind sector for these sensors is 0°-360°, or all directions.

2.3.1.4 SLC 41

The wind sensors at SLC 41 are mounted at 230 ft on two of the four lightning protection towers surrounding the launch pad. The towers are triangular and of lattice construction, and would experience the same issues of disturbed flow through the towers as with scaffold construction. The launch complex is orientated 10°-190°, just 10° off true north and south. The four towers surround the pad with two on the north side and two on the south side. The wind sensors are on the northwest and southeast towers. Figure 4a is a Google Earth image of the lightning protection towers and Figure 4b shows the individual tower shape and orientation, and the location of the sensors on the towers.

Based on data provided by the 45 WS, the AMU assumed the towers were equilateral triangles and that one side of each sensor tower was parallel to the pad orientation. The AMU also assumed that the sensor booms extended out from the point of the triangles and not parallel to one side. Using these assumptions, the sensor on the northwest tower is on the triangle point directed at 280° and the sensor on the southeast tower is on the point directed at 220° (Figure 4b). The upwind directions for the northwest sensor, including along the sides of the tower, would be 130° through 70° (clockwise), and for the southeast sensor 70° through 10° (clockwise).

If a 22°-24° buffer similar to that for the scaffold towers is introduced, there would be a sector to the northeast that would not be upwind from either sensor. For example, a 20° buffer along each edge would create an upwind sector of 150°-50° (southeast through northeast, clockwise) for the northwest sensor and 90°-350° (east through north-northwest) for the southeast sensor. This leaves a 40° sector from 50°-90° (northeast to east) that would be downwind from both sensors and, therefore, not included in the analysis. The winds from this sector have had the lowest peak wind thresholds for some of the launches, making it a critical sector from which to have reliable wind observations. The AMU used the upwind sectors without a buffer so that all directions would be included in the analysis. This may have introduced error into the statistics.

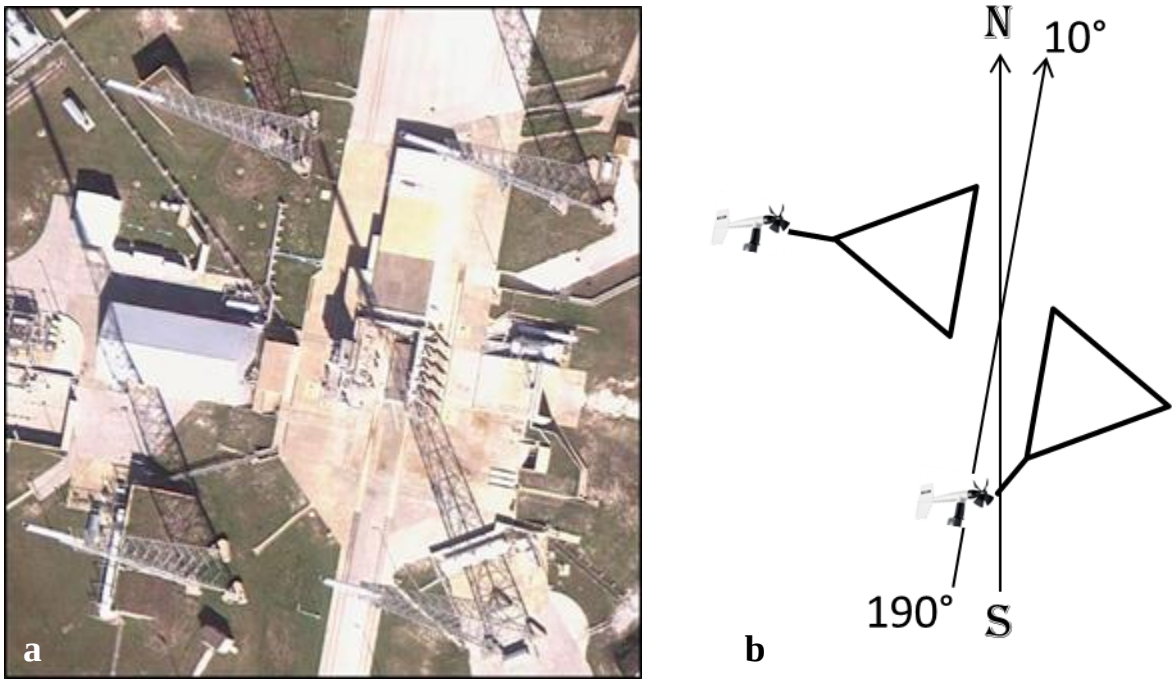

Figure 4. a) Google Earth image of the lightning protection towers at SLC 41 and b) tower shape and orientation, and sensor location. The image in 4a is oriented to true north and the drawing in 4b is not to scale.

2.3.2 Onshore/Offshore Flow

The AMU determined the onshore and offshore flow sectors within the upwind sectors for each sensor, shown in Table 3. The coastline nearest Towers 6, 108 and 110, and SLCs 39 and 41 is oriented approximately 315°-135°, or northwest to southeast (Figure 1). Following Bauman (2010), the onshore sector for these towers was 316°-135° and the offshore sector was 136°-315°.

Table 3. The LCC wind towers and sides, the upwind sectors, and the onshore and offshore sectors within the upwind sectors. All direction ranges are clockwise.

Tower and Side	*Upwind Sector*	*Upwind Onshore*	*Upwind Offshore*
0020 NW	226°-45°	—	226°-45°
0021 SE	46°-225°	46°-225°	—
0061 NW	204°-68°	316°-68°	204°-315°
0062 SE	23°-248°	23°-135°	136°-248°
SLC 41 NW	130°-70°	316°-70° 130°-135°	136°-315°
SLC 41 SE	70°-10°	316°-10° 70°-135°	136°-315°
108 SE	23°-248°	23°-135°	136°-248°
1101 NW	204°-68°	316°-68°	204°-315°
1102 SE	23°-248°	23°-135°	136°-248°
0393 NW	0°-360°	316°-135°	136°-315°
0394 SE	0°-360°	316°-135°	136°-315°
0397 NW	0°-360°	316°-135°	136°-315°
0398 SE	0°-360°	316°-135°	136°-315°

The upwind sectors used for Tower 2 were different than the other towers to the north (Figure 1). The coastline just south of Tower 2 is oriented 45° to 225°. The LWOs consider this the dividing line for onshore and offshore flow at this tower (Joel Tumbiolo, personal communication). For the northwest sensor, the upwind and offshore sector is 226° through 45° (clockwise); for the southeast sensor, the upwind and onshore sector is 46°-225°. These are 180° sectors as opposed to the 225° sectors described previously. Onshore for the northwest sensor would be from the two sectors 46°-68° and 204°-225°, which are 22° and 21° wide, respectively. This results in a 43° onshore flow sector that is too small to derive meaningful onshore statistics for the northwest sensor. The same argument can be made for offshore flow at the southeast sensor.

2.3.3 Speed Filter

A speed filter was applied to remove all records in which the mean speed was < 5 kt. Speeds in this range are not operationally significant and were not associated with operationally significant peak winds. The LWOs stated that the lowest peak LCC threshold for any of the vehicles is 20 kt. The lowest mean speed associated with a peak of 20 kt in the entire database was 5 kt. Therefore, all records with mean speeds ≥ 5 kt were used in the analysis.

2.3.4 Stability

One of the suggestions for future work in the Phase III final report (Crawford 2010) was to stratify the data by stability. Merceret and Crawford (2010) found that tropical storm and non-tropical storm gust factors could not be compared properly without first stratifying the non-tropical storm data by this parameter. They confirmed the findings of previous studies (e.g. Monahan and Armendiraz 1971, Paulsen and Schroeder 2005) that stability is an important factor in the magnitude of peak winds.

2.3.4.1 Local Stability at the Towers

Through consultation with Dr. Merceret at the KSC Weather Office and Mr. Roeder of the 45 WS, the AMU chose the Richardson number as the stability parameter for stratifying the data. The AMU calculated the gradient and bulk Richardson numbers (R_i and R_B) for each level on Towers 2 and 313 collected in January, all years in the POR. The details of the calculations are in the appendix.

Stull (1988) states that flow becomes turbulent when $R_i < 0.25$. Using this criterion, the AMU determined the percentage of unstable values for each hour of the day at Towers 2 and 313, shown in Table 4. There was a clear diurnal signal. In January, the sun rises locally at 0700-0715 EST and sets at 1745-1800 EST. In Table 4, the day hours and their associated unstable frequencies in percent between sunrise and sunset are in the left three columns, and the same values for the night hours between sunset and sunrise are in the right three columns. The percentages increased quickly after sunrise to 99-100% between 1000 and 1600 EST, and then dropped quickly to overnight values by sunset. The overnight values remained steady with a slight increase in the midnight hours between 1100 and 0300 EST in both towers, and values were 10-15% lower at Tower 313.

The quick increase to 100% was likely due the surface-level instability created by solar heating of the ground. The cause of the slight increase in the steady values around midnight is unclear. Nonetheless, the percentages of unstable cases were still higher than expected for the overnight. Unstable R_i values occurred both day and night even when the region was under the influence of a strong, stable, high pressure center. The results for R_B were almost identical. Based on these results, the AMU concluded that the tower data could not be used to determine the local stability at the towers.

Table 4. Hourly frequencies in percent of $R_i < 0.25$ for Towers 2 and 313 in January 1995-2010.

Hour EST (UTC)	*2*	*313*	***Hour EST (UTC)***	*2*	*313*
07 (12)	73	54	**19 (00)**	71	57
08 (13)	82	63	**20 (01)**	70	57
09 (14)	97	90	**21 (02)**	71	59
10 (15)	100	99	**22 (03)**	71	61
11 (16)	100	100	**23 (04)**	73	63
12 (17)	100	100	**00 (05)**	76	62
13 (18)	100	100	**01 (06)**	78	64
14 (19)	99	100	**02 (07)**	76	62
15 (20)	99	100	**03 (08)**	77	62
16 (21)	99	100	**04 (09)**	74	58
17 (22)	94	96	**05 (10)**	74	57
18 (23)	78	64	**06 (11)**	74	58

2.3.4.2 Areal Stability from the Soundings

Unable to use R_i or R_B to determine local stability at the towers, the AMU pursued using the CCAFS soundings to determine areal boundary layer stability. The AMU sent the QC-d soundings to Mr. Kienzle of ENSCO's GeoSystem Solutions (GS) Division to calculate the mixed layer (ML; Stull 1988) height using algorithms he developed for transport and diffusion models. The AMU intended to use the ML height as the proxy for the height of the boundary layer in determining the areal stability over KSC and CCAFS. Mr. Kienzle delivered the ML data to the AMU along with supporting documentation, which revealed a difference between the way the Richardson number was calculated for the ML data and the formula the AMU used for the tower data. Mr. Kienzle determined that the version of the Richardson number he used assumed a wind speed of 0 at the surface. He modified the code with a new version of the Richardson number that uses the wind speed at the first layer of the sounding and began testing the algorithm. Testing had not been completed by the end of June, but the AMU had to move forward with the task in order to complete it by the 30 September deadline. The AMU met with Mr. Roeder of the 45 WS to discuss the issues, and he directed the AMU to calculate the climatologies and probabilities using the upwind onshore/offshore stratifications.

2.3.4.3 Solar Parameter

The gust factor means and standard deviations shown in Figure 5 followed similar trends as the speed climatologies: relatively constant values during the night, increasing values after sunrise to mid-day, and decreasing through sunset. The onshore mean values were consistently less than the offshore values, but the standard deviations were similar. Dr. Merceret compared the gust factor curves to a solar parameter for January. This parameter varies from 0 to 1 and depends on the sun angle for each hour and day of year (http://www.gcstudio.com/suncalc.html). Figure 5 shows the solar parameter hourly curve calculated for 15 January (mid-month). There is a visual correlation between the GF and solar curves.

Dr. Merceret explored this apparent relationship between the solar parameter and the gust factor means and standard deviations to determine if it could be used as a proxy for stability. He found good fits with linear regression between the solar parameter and the gust factor means and standard deviations. However, in a comparison between the forecasting capability of the solar parameter vs. the Gumbel distribution described later in this report, Dr. Merceret found the performance of the two methods was similar, with the Gumbel distribution performing slightly better.

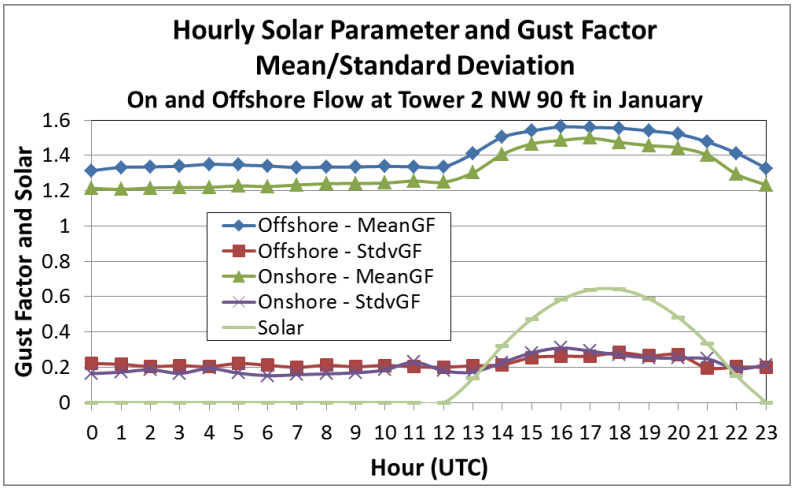

Figure 5. Hourly gust factor means and standard deviations at the 90-ft NW sensor on Tower 2 in January, and the solar parameter curve for January 15.

3. Climatologies and Probabilities

The climatologies and probabilities described were calculated using similar methods as in Phases I (Lambert 2002) and III (Crawford 2010), but with the added onshore/offshore stratification and filtering of records with mean speeds < 5 kt. The QC-d observations were imported into the S-PLUS® software package for processing, and the resulting statistics were then imported into Excel for display and GUI development.

The AMU calculated diagnostic and prognostic peak wind speed probabilities for given mean wind speeds. The diagnostic probabilities reveal the characteristics of the peak speeds observed during the same 5-min period as their associated mean speeds. The prognostic probabilities show peak speed behavior in a set time period past the 5-min mean observation.

3.1 Climatologies

The AMU modified scripts from the Phase III task to calculate the climatologies for the new period of record. The climatologies are the hourly means (μ) and standard deviations (σ) of the 5-min mean and peak speeds for onshore and offshore flow. The hourly onshore/offshore μ and σ of the 5-min mean and peak winds were calculated for each month and sensor. The values were calculated using the 12 5-min winds in each hour for all days in each month and all years in the POR. A sample of these climatological values is given in Figure 6, which shows the hourly peak and mean speed climatologies and the number of observations used to calculate them for the 54-ft sensor on the northwest side of Tower 6 in April.

The differences in the diurnal trend of μ between onshore and offshore flow can be seen in Figure 6a. The local sunrise in April is 1045-1115 UTC (0545-0615 EST), and sunset is 2340-0000 UTC (1840-1900 EST). The offshore speeds increased quickly after sunrise and continued increasing through the day. They began decreasing approximately three hours before sunset and continued decreasing through sunrise. The decrease after sunset was more gradual than before sunset. The total diurnal change was ~ 7 kt for the peak speeds and ~ 4 kt for the mean speeds. The daytime increase was likely caused by mixing down of higher momentum winds aloft by convective elements created by daytime heating of the upstream land surface. The late afternoon/nighttime decrease may have been due to the reduction in surface heating convection during the afternoon and a nocturnal inversion that may have formed and intensified slowly after sunset and through the night. In contrast, the onshore values remained relatively steady, dipping slightly just before sunrise, and increasing by only 1-2 kt during the day. With only a short fetch of land upstream, the onshore winds would be influenced only minimally by land-heating induced convection. The offshore diurnal pattern was similar in all sensors and months, but the onshore pattern showed variations between the months. For example, in October for the same sensor in Figure 6 (not shown), the onshore peak winds were always higher than the offshore values and the onshore values decreased slightly after sunrise.

The number of occurrence curves in Figure 6b show more occurrences of offshore flow at night and more occurrences of onshore flow during the day. The increase in offshore flow events at night could reflect the occurrence of the land breezes in the overnight hours known to occur over KSC/CCAFS, and the increase in onshore flow events during the day could be a result of the increase in sea breeze events starting in April.

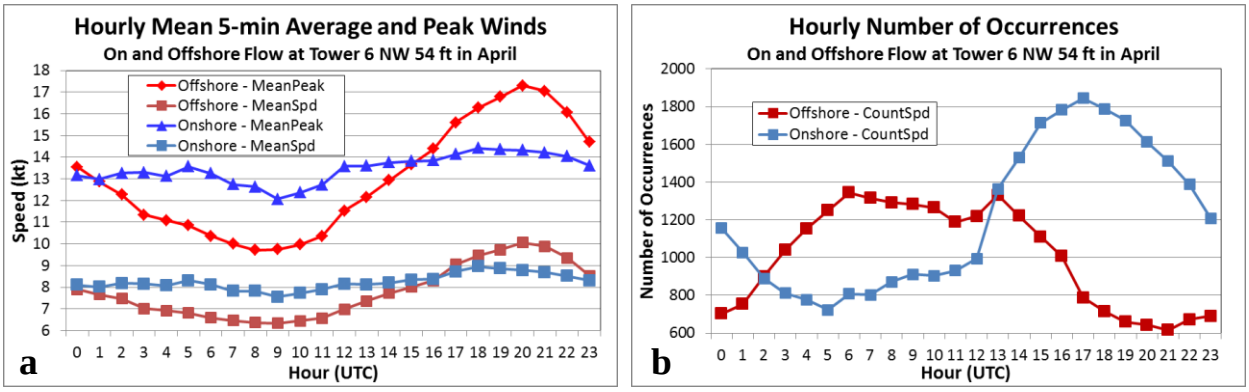

Figure 6. The hourly onshore and offshore a) speed climatologies and b) number of occurrences for the northwest sensor of Tower 6 in April. The legend shows the curve colors for μ of the 5-min peak (MeanPeak) and mean speeds (MeanSpd), and σ of the peak (StdvPeak) and mean speeds (StdvSpd). The offshore curves are in shades of red and the onshore curves are shades of blue.

3.2 Probabilities

As in Phase III, the AMU calculated the probability of meeting or exceeding a specific peak speed threshold given a 5-min mean speed. For every knot of mean wind speed, a range, or distribution, of peak speeds was observed over the 16-year POR. The distributions were used to create the diagnostic and prognostic empirical probabilities. As in Phase III, the Gumbel distribution was fit to the diagnostic empirical distributions. This serves a two-fold purpose: 1) to smooth over variations in distributions, and 2) estimate probabilities of peak speeds beyond the range of the observations in the POR. In Phase III, the AMU concluded that no single parametric distribution could be used to model the prognostic probabilities (Crawford 2010), therefore it was not done in this phase.

3.2.1 Diagnostic Empirical Distributions

The AMU stratified the peak winds by 5-min mean wind speed in 1-kt intervals and created empirical probability density functions (PDFs) of the peak winds for each month and sensor on each tower at each height. The PDF was calculated by dividing the number of observations of each individual peak speed in the distribution by the total number of observations associated with the mean wind speed. This produced a value representing the frequency of occurrence of each peak speed in the distribution. The sum of the frequencies in a PDF is, therefore, 1. Figure 7 shows the PDFs for onshore flow at Tower 110 northwest 204-ft sensor in October. Only the even mean speed PDFs in the range 6-34 kt are shown to keep the chart uncluttered. Each curve represents a mean speed and each point on the curves represents the frequency of occurrence of the peak speed on the horizontal axis.

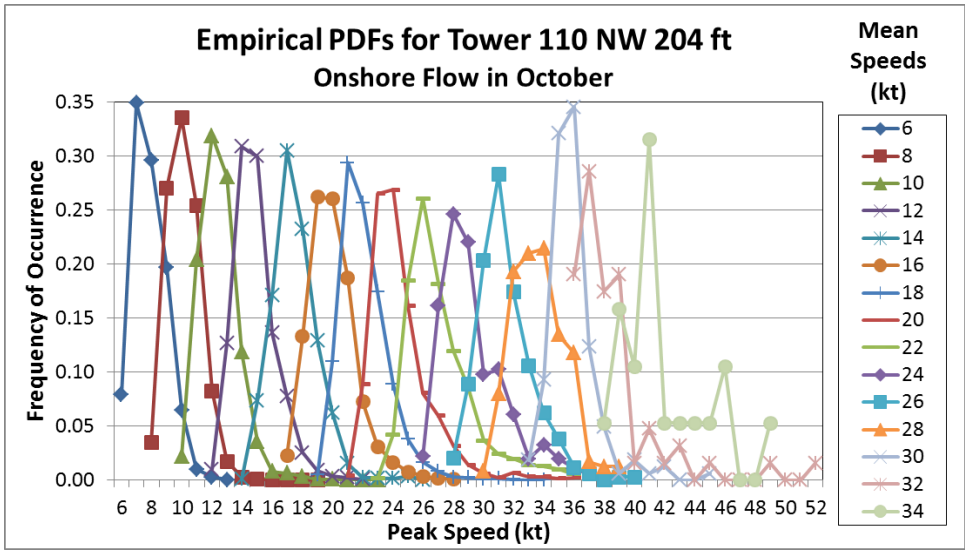

Figure 7. The empirical PDF curves for onshore flow at the Tower 110 northwest 204-ft sensor in October. Each curve represents a mean speed whose symbol and color are shown in the legend at right. The values along the curve are the peak speeds given in the horizontal axis. The vertical axis shows the frequency of occurrence of each peak speed in each PDF.

A cumulative distribution function (CDF) was created by integrating the PDF values from the lowest to highest peak speeds in the distribution. The CDF specifies the probability that a peak speed will not exceed a certain value (Wilks 2006). The 45 WS forecasters need to know the opposite: the probability of the peak speed meeting or exceeding a specific LCC value. To create the desired values, the AMU calculated complementary CDFs (C-CDFs), given by 1 – CDF. The peak speed C-CDFs derived from the PDFs in Figure 7 are shown in Figure 8a. Each symbol on a mean speed curve corresponds to a peak speed on the horizontal axis and a probability of meeting or exceeding that peak speed on the vertical axis. Figure 8b shows the total number of observations in each C-CDF. The value falls steadily from 1814 at 10 kt to 13 at 34 kt. The under-sampling of the 34-kt mean and associated peak speeds in the distribution resulted in an irregular curve in both Figure 7 and Figure 8a. This shows that a small number of observations can create erroneous probabilities and would be misleading to a forecaster.

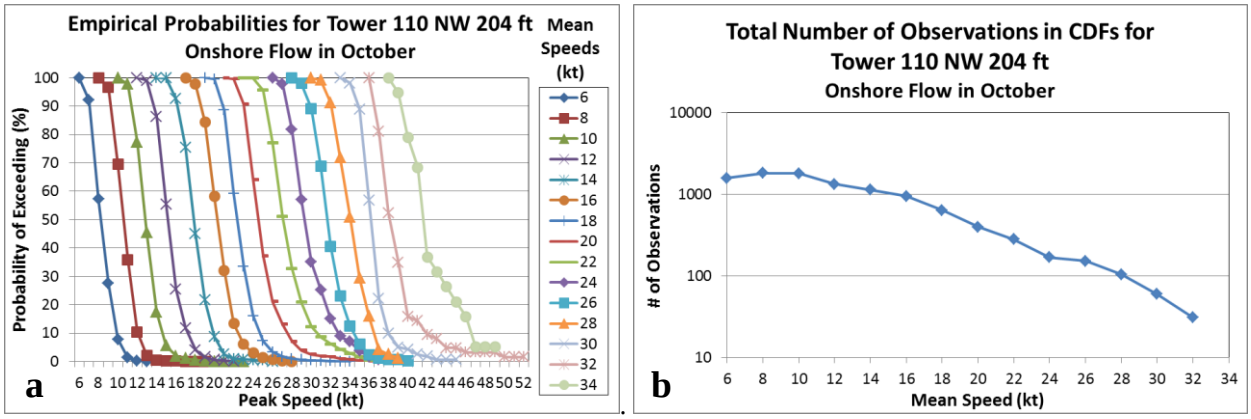

Figure 8. a) The C-CDF curves for onshore flow at the Tower 110 northwest 204-ft sensor in October, and b) the number of mean speed observations used to create the curves in 8a. Each curve in 8a represents a mean speed whose symbol and color are shown in the legend at right. The vertical axis in 8a is the probability of meeting or exceeding a peak speed in percent, and the vertical axis in 8b is the logarithmic number of observations.

3.2.2 Diagnostic Parametric Distributions

As stated earlier in this report, there are two reasons for fitting parametric distributions to empirical distributions as defined in Wilks (2006). The first is to smooth over the variations in empirical distributions due to possible under-sampling of a specific peak gust. The second is to estimate probabilities of peak gusts associated with mean wind speeds outside the range of the observations in the data sample. The assumption inherent in the second reason is that the parametric distribution would also represent the peak wind distributions for rarely or as-yet unobserved mean wind speeds. Determining the validity of this assumption was difficult for the data in this study due to very small or non-existent sample sizes for such speeds.

Fitting the C-CDFs with the proper parametric distribution was necessary for calculating the appropriate probability values, especially for extreme values that were observed only occasionally. In Phase III, the AMU used the Gumbel distribution as requested by the 45 WS since it had been proven to be the best fit for winds from the KSC/CCAFS wind tower network in studies conducted at Marshall Space Flight Center. Wilks (2006) identifies the Gumbel as an often-used extreme value distribution and, as such, is appropriate for peak winds. Detailed descriptions of the Gumbel equation and how it was applied to the data were given in the Phase III final report (Crawford 2010, Section 3.2.2).

In Phase III (Crawford 2010), the Gumbel distribution could not be fit to higher mean speed distributions because of too few observations. The AMU developed a method to determine the highest mean speed whose distribution could be fitted. A detailed description of this method and how it was developed is given in the Phase III final report (Crawford 2010, Section 3.2.2). The algorithm isolated the mean speed distributions with ≥ 100 and ≤ 400 observations, then chose lowest speed with the highest change in the Gumbel parameters from the previous speed as the cutoff. The Gumbel distribution was fit to all distributions with mean speeds less than the cutoff speed.

Figure 9 shows the resulting Gumbel C-CDFs for onshore flow at the Tower 110 northwest 204-ft sensor in October, the fitted counterpart to the empirical C-CDFs in Figure 8a. The range of mean speeds with 100-400 observations was 20-28 kt. As with previous figures, only the even mean speed C-CDFs are shown. The maximum mean speed in the chart is 26 kt, but the algorithm determined the highest fitted mean speed distribution is 27 kt.

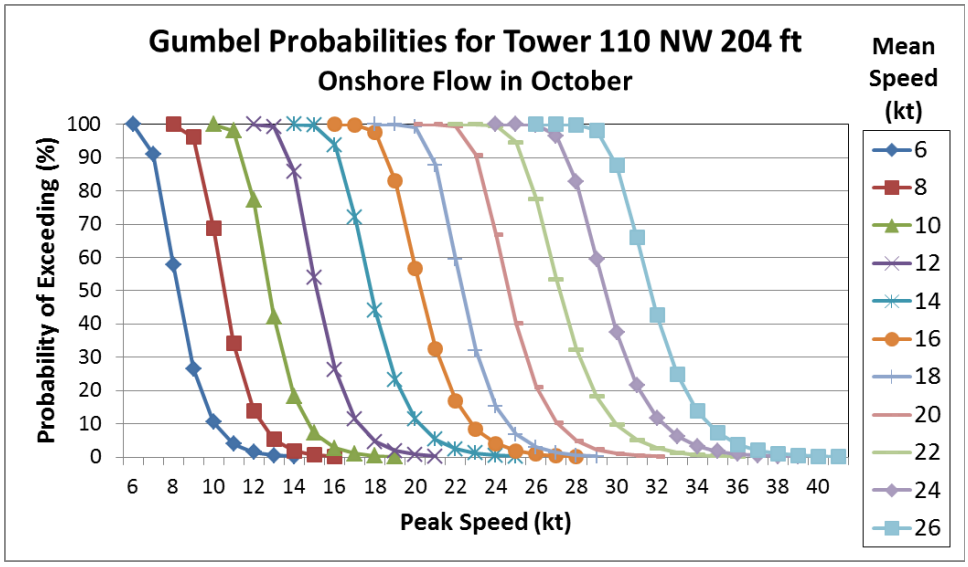

Figure 9. The Gumbel C-CDF curves for onshore flow at the Tower 110 northwest 204-ft sensor in October. Each curve represents a mean speed whose symbol and color are shown in the legend at right. The values along the curve are the peak speeds given in the horizontal axis. The vertical axis shows the probability of meeting or exceeding a peak speed based on the mean speed.

3.2.3 Empirical Prognostic Probabilities

The prognostic probabilities provide the probability of meeting or exceeding a specified peak speed within a specified time period after a 5-min mean speed observation. The time periods requested by the 45 WS were 2, 4, 8, and 12 hours, the same as in Phase III. Due to the extra time needed to modify the algorithm due to the new upwind/≥ 5kt filters and onshore/offshore stratifications, the AMU was able to complete the 2- and 4-hour probabilities, but not the 8- and 12-hour probabilities.

3.2.3.1 Phase III Data Processing

The data processing algorithm used in Phase III is summarized here to assist in understanding the algorithm used in this work. The AMU developed a re-sampling technique to prepare the data for calculating the prognostic probabilities that used all 5-min mean and peak speeds in the data set by processing them an hour at a time. This was done to see if there would be enough data to create hourly probabilities. Figure 10 demonstrates how the data were collected for the 5-min mean speeds surrounding 0000 UTC. The 12 mean speeds in the 30 min intervals before and after the central time of 0000 UTC represent the mean speeds for that hour. This time period, 2330–0025 UTC, is highlighted in blue in Figure 10. The brackets above the timeline encompass the range of times from which the peaks are drawn for the first and last times in the blue area. The peak speeds associated with the mean speed at 2330 UTC were taken from the time period 2335-0125 UTC. The peaks associated with the mean speed at 0025 UTC were taken from the time period 0030-0220 UTC. This technique assured that every mean speed in the data set was used, but also meant that the same peak speed would be used, or re-sampled, in multiple distributions. The same procedure was followed for every 5-min mean speed in the data set. For the 2-hour prognostic probabilities, this resulted in 23 peak speeds associated with each mean speed. Each set of 23 peak values was binned with its associated mean speed. Note that for the 4-hour probabilities, there would be 47 peak speeds with each mean speed.

The 2-hour sets, identified by a mean speed and 23 peak speeds, were combined with sets having the same mean speed. For example, the first step in the procedure would create 360 1-mean/23-peak sets for a specific hour in a month with 30 days. The sets with identical mean speeds were combined. If there were 20 different mean speeds in the set of 360, the end result would be 20 sets with a large number of peak speeds in each. These distributions were used to calculate the empirical C-CDFs for each hour/month/tower/height. Each mean speed then had a distribution of peak speeds associated with it. As described in the Phase III report, the AMU concluded that there were not enough data to stratify by hour, or any time period less than 24 hours, and properly model the higher wind speeds important to operations. Therefore, the processed hourly data were combined prior to calculating the prognostic probabilities.

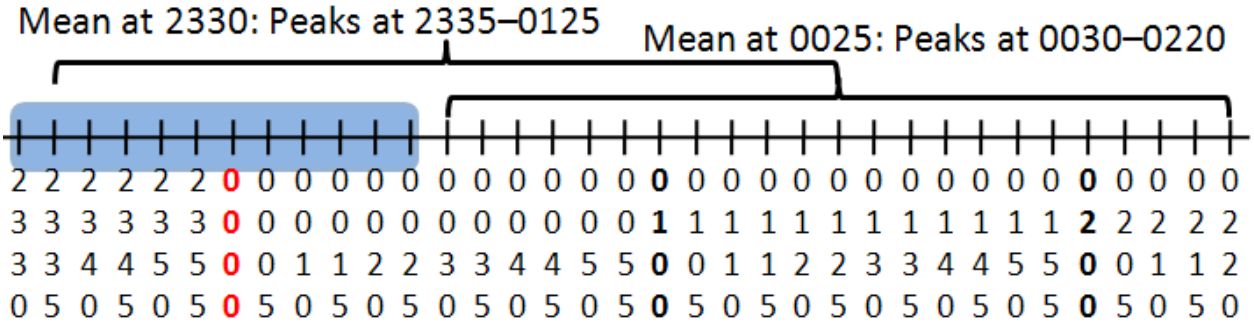

Figure 10. Timeline showing how the data for the 2-hour probabilities at 0000 UTC were collected. The times highlighted in blue represent the set of 5-min mean speeds. The brackets above the timeline represent the range of times over which the 5-min peaks were collected for the first and last mean speed observations in the blue shaded area. The time of interest, 0000 UTC, is highlighted in red.

3.2.3.2 Phase IV Data Processing

The complicating factors for processing the Phase IV data were the onshore/offshore stratifications and upwind/≥ 5 kt filters that created time gaps in the data files. Even though the data were stratified by tower sensor and month in Phase III, all times were available, or indicated as missing if not available, and sequential. The algorithm just counted the number of records in the file to get the mean speeds 30 minutes before and after each hour and for the required number of peak speeds following a mean speed. In the Phase IV data, records could be missing in the mean speeds surrounding the hour and/or in the peak speeds for each mean.

For example, assume the data are for onshore flow, and onshore flow did not begin until 2345 UTC in Figure 10. The data from 2330-2340 UTC would not be in the file, but other records from earlier times would be in their place. The same would be true for the range of peak speeds. If the flow regime changed within the 23 observations needed for the 2-hour distributions, those records would not be in the file and, in their place, would be replaced by later times that should not be included. The peak speed times for a mean speed time of 2345 are 2350-0140 UTC. If, at 0115 UTC, the flow changed or the direction was no longer upwind or the mean speed dropped below 5 kt and did not change back until after 0140 UTC, the records at these times would not be in the file and records with times later than 0140 would be in their place. Such values should not be included in the peak speed group.

To make sure that the onshore probabilities were created from data within the correct time periods, the AMU modified the algorithm to insure the times of the records used for the probabilities were properly matched. The algorithm checked the six records before and five records after the hour being analyzed to ensure the proper mean speeds were being chosen, and then checked the times in the 23 peak speed observations following each correct mean speed to make sure the times of the observations were within 2 hours of the mean speed. This resulted in some hours having less than 12 mean speed observations and some 2-hour peak speed ranges having less than 23 observations. The result is that the onshore prognostic probabilities were created with only onshore values and the offshore probabilities created with only offshore values within the appropriate time periods.

3.2.3.3 Empirical Prognostic C-CDFs

The empirical 2-hour prognostic probabilities for onshore flow at the Tower 108 southeast 54-ft sensor in March are shown in Figure 11. These are interpreted as the probability of meeting or exceeding a specific peak speed over the next two hours given the 5-min mean speed. The curves for the even mean speeds only are shown to keep the chart uncluttered. The C-CDF curves for mean speeds higher than 20 kt were not smooth as a consequence of the low number of observations used to create them. There were 709 observations used to create the C-CDF for 20 kt. The number of observations for each subsequent speed dropped to 139 at 22 kt and 83 for 24 kt. Note also that the peak speed probabilities begin at 5 kt. It is possible, and more likely at higher mean speeds, for the peak speeds to decrease from the mean value over any time period other than at the same time as the mean speed observation.

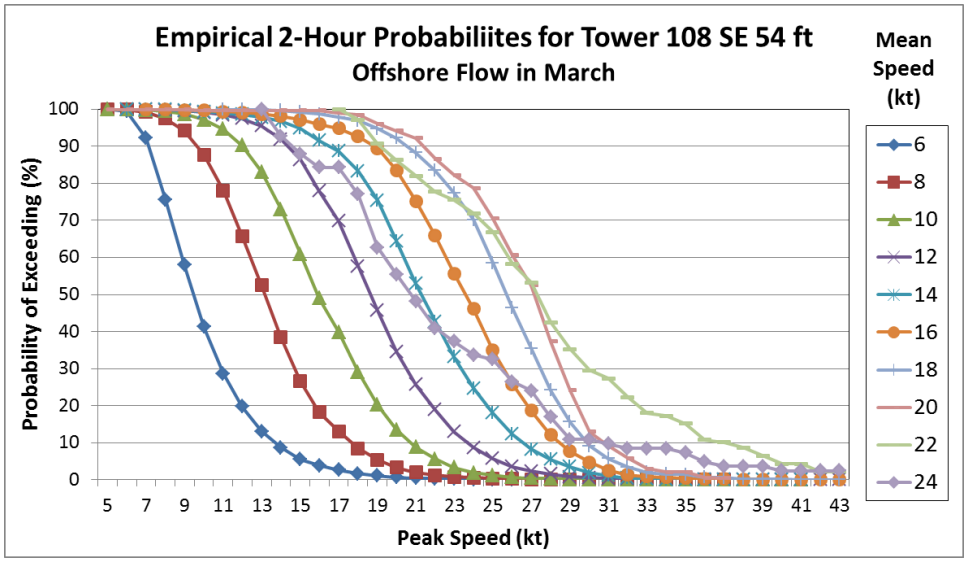

Figure 11. The empirical 2-hour C-CDF curves for offshore flow at the Tower 108 southeast 54-ft sensor in March. Each curve represents a mean speed whose symbol and color are shown in the legend at right. The values along the curve are the peak speeds given in the horizontal axis. The vertical axis shows the probability of meeting or exceeding a peak speed based on the mean speed.

4. Graphical User Interface

The AMU modified the GUI developed in Phase III to accommodate the new onshore/offshore stratifications in Phase IV. This GUI was delivered to the 45 WS during development to test and make suggestions for modifications, all of which were incorporated. This ensured that the end product met their needs, was easy to use, and produced useful information in a readable format.

4.1 Initial Form

The GUI starts automatically when opening the file LCC.PK.WIND.GUI.P4.xlsm. The initial form has two tabs, one for the climatologies and the other for the probabilities. Figure 12a shows the "Climatology" tab and Figure 12b shows the "Probability" tab. On both tabs, the user chooses the tower, sensor height, month, and flow regime of interest. The tower must be chosen before the height because the choice of heights in the drop-down list is limited to the heights on the tower displayed in the "Tower" text box. The option button choice for onshore flow in both tabs is grayed out for the Tower 2 northwest sensors since onshore statistics were not calculated for this side (section 2.3.2). The same is true for offshore flow when the southeast side of Tower 2 is chosen. The specifics of the other choices on each tab are discussed in Sections 4.2 and 4.3.

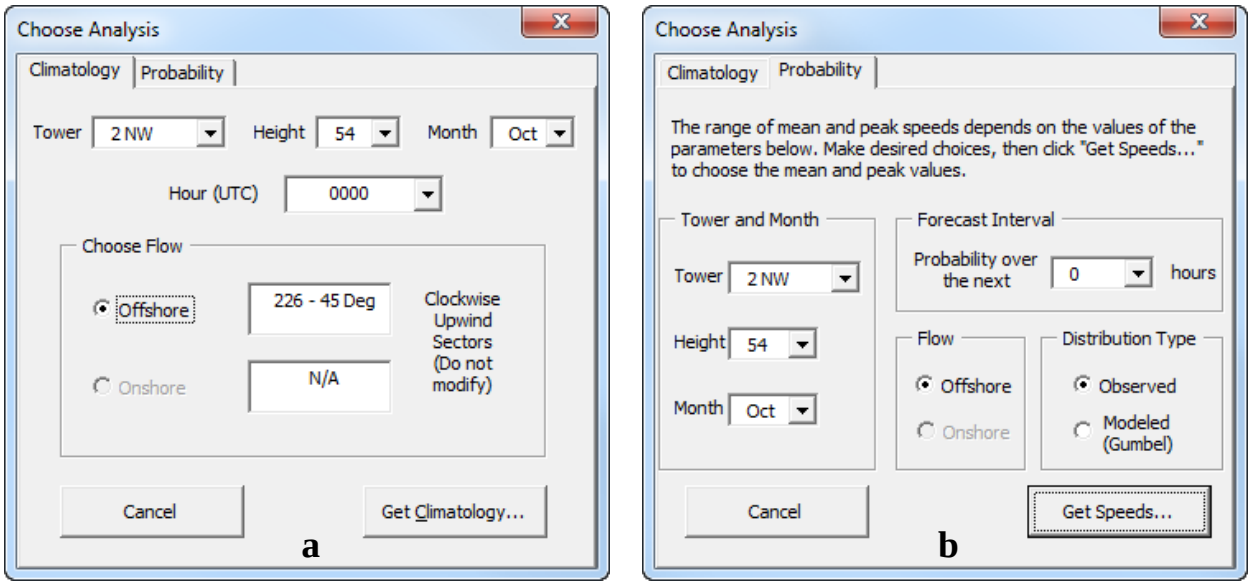

Figure 12. The Climatology (a) and Probability (b) tabs in the initial GUI form.

4.2 Climatology

After choosing tower, height, and month on the "Climatology" tab, the next step is to choose the desired hour and flow regime. The hours are in UTC and the direction sector(s) for each flow regime are given in text boxes to the right of their respective regime names. The flow sector values cannot be changed. After all choices are made, the user will click the "Get Climatology..." button and an output form with the retrieved information will be displayed.

Figure 13 shows the "Climatology" tab (a) and the "Requested Climatology" output form (b). The "Tower" drop-down list is shown in Figure 13a with 41 NW chosen, referring to the northwest tower at SLC 41 (Figure 1). After choosing this tower, "Height" changes to 230 ft automatically. That is the only sensor height on this tower. For other towers with two heights, the choices will be in a drop-down list. The "Month" is October, the "Hour" is the default 0000 UTC, and the flow regime is onshore. See sections 2.3.1.4 and 2.3.2 for a description of the upwind onshore sectors for this tower.

The top portion of the output form in Figure 13b reiterates the information chosen in the "Climatology" tab (Figure 13a). The climatology values are displayed in the "Wind Statistics" section. This includes the average, standard deviation, and number of observations for the mean and peak wind speeds. Next to this section is the "Choose Another Analysis" button used to close the output form and return the user to the initial tab. The notice at the bottom reminds users that the values displayed were calculated from historical data, not currently observed data, and should not be used as an absolute forecast for future winds.

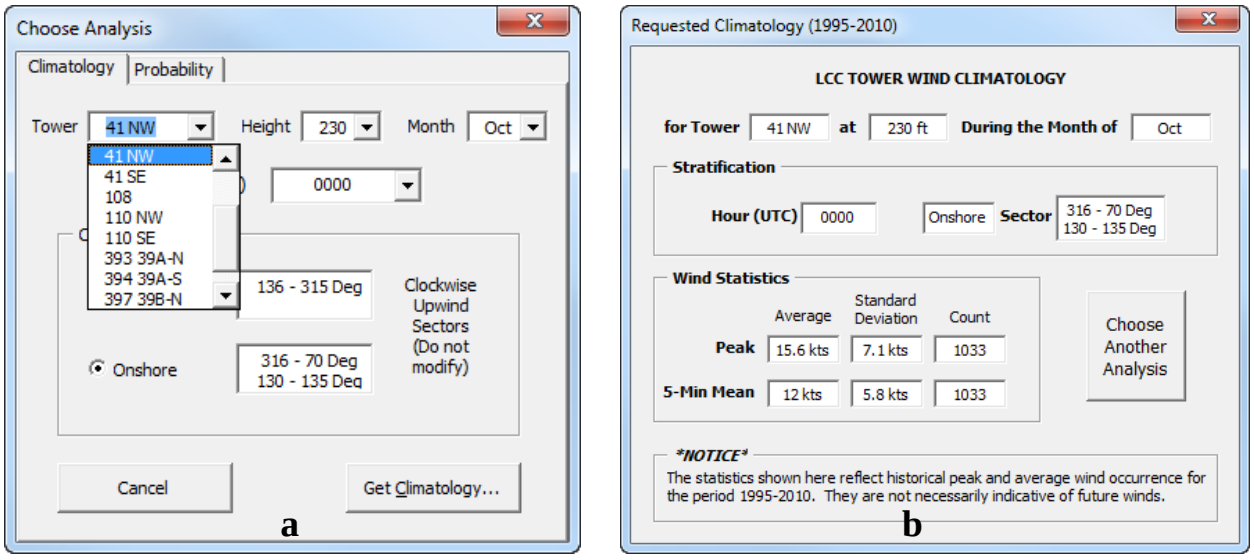

Figure 13. a) The "Climatology" tab of the initial GUI with the height drop-down list displayed, and b) the "Requested Climatology" output form showing the 0000 UTC mean and peak wind speed climatology values for onshore flow at the SLC 41 NW 230-ft sensor in October.

4.3 Probability

After choosing the tower, height and month on the "Probability" tab, the user will choose the "Forecast Interval" and "Distribution Type". The "Forecast Interval" choices are the diagnostic (0 hours) or prognostic (2 or 4 hours) probabilities. When 0 is chosen, the user can choose the observed diagnostic probabilities or those modeled with the Gumbel distribution, as described in section 3.2.2. Figure 14a shows the "Probability" tab with 0 hours for the "Forecast Interval". "Observed" and "Modeled (Gumbel)" are active in the "Distribution Type" section, meaning either can be chosen. Figure 14b shows the "Forecast Interval" drop-down list with the 4-hour prognostic time period chosen. Note that "Modeled (Gumbel)" in the "Distribution Type" section is grayed out, indicating that it cannot be chosen. Recall from the beginning of section 3.2 that the prognostic probabilities were not modeled with a parametric distribution and only the observed probabilities are available in the GUI.

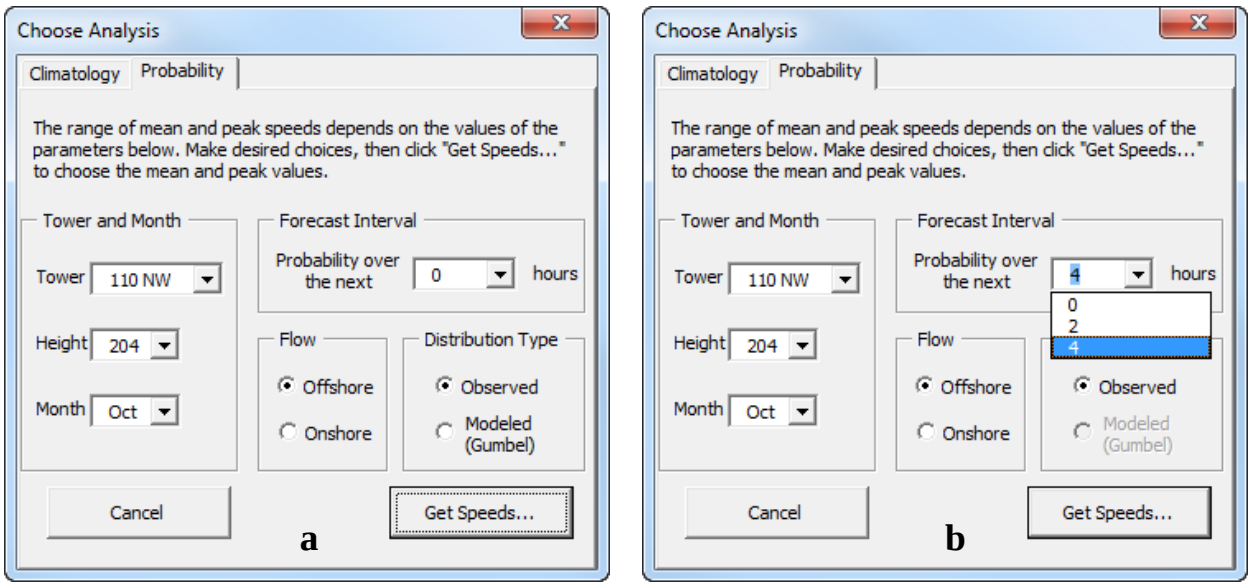

Figure 14. The initial Probability tab showing the choices for the (a) diagnostic and (b) prognostic probabilities.

Once all choices are made in the "Probability" tab, the user clicks the "Get Speeds..." button and the "Choose Mean and Peak" form in Figure 15 is displayed. It allows the user to choose the mean and peak speeds of interest. The choices in the initial form (Figure 14) determine the range of mean speeds in the drop-down list, and the choice of mean speed determines the range of peak speeds. Figure 15 shows the form after 15 kt and 20 kt were chosen as the mean and peak, respectively, from drop-down lists. The "New Parameter Values" button takes the user back to the "Probability" tab to change the input parameters if desired. Clicking the "Get Probability…" button displays the output form with the desired probability values.

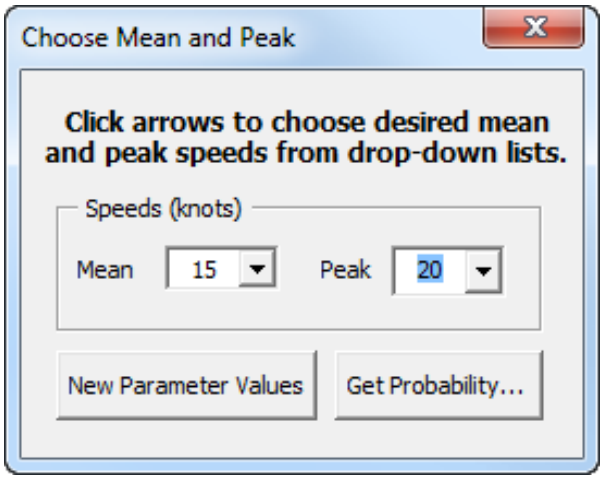

Figure 15. The form to choose the mean and peak speed of interest, displayed after clicking "Get Speeds..." in the Probability tab (Figure 14).

Figure 16a shows the "Choose Mean and Peak" form output when a prognostic value for "Forecast Interval" in Figure 14b is chosen. For the diagnostic probabilities, it is not possible to have a peak speed lower than the mean since the peaks are from the same 5-min period as the mean. However, it is possible to have lower peak speeds over a time period after a mean is observed, in this case within four hours after the mean. The top portion of the peak speed drop-down list in the "Choose Mean and Peak" form is shown to demonstrate this. In Figure 16a, 10 kt was chosen for the peak speed. This is less than the chosen mean speed of 15 kt. When this happens, the "Peak Wind Value Warning" form in Figure 16b is displayed when the "Get Probability..." button in Figure 16a (behind the drop-down list) is clicked. It lets the user know that a peak speed less than the mean was chosen and provides the choice of proceeding or not. Clicking the "No" button will close the warning form and return the user to the "Choose Mean and Peak" form where a new peak value can be chosen.

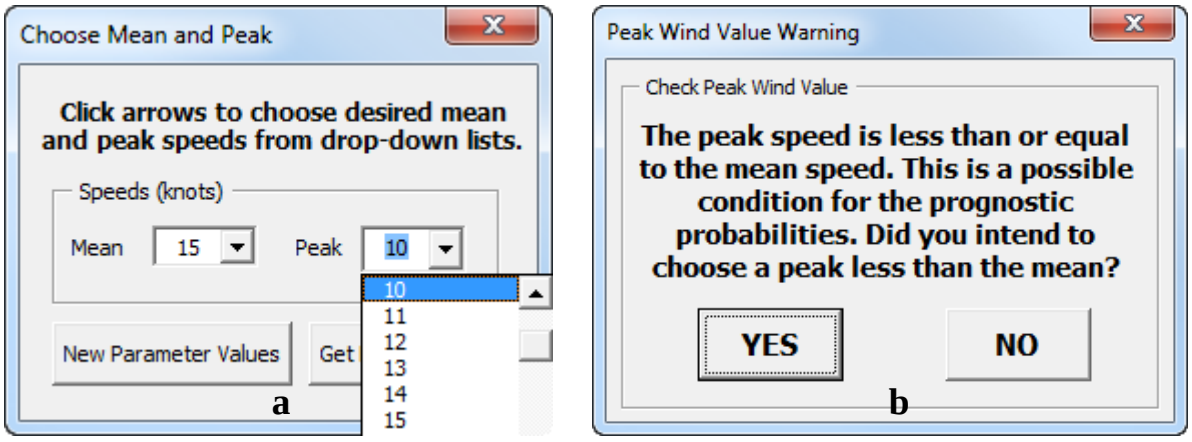

Figure 16. a) The "Choose Mean and Peak" form displayed after the Forecast Interval is set to one of the prognostic probability periods, in this case 4 hours (Figure 14b), and b) the warning form displayed when the peak speed chosen is less than the mean speed.

When "Get Probability..." in the "Choose Mean and Peak" form or "Yes" in the warning form is clicked, the "Requested Probability" output form is displayed. User-input from the first two forms is repeated at the top, and the probability is displayed in large font. Figure 17 shows the results from the choices in Figure 14b and Figure 15. The notice at the bottom left is similar to the statement on the climatology output forms. It reminds users that the values displayed were calculated from historical data, not currently observed data, and should not be used as an absolute forecast for future winds. The "Retrieve Another Peak Speed Probability" button closes the form and returns the user to the "Choose Mean and Peak" form.

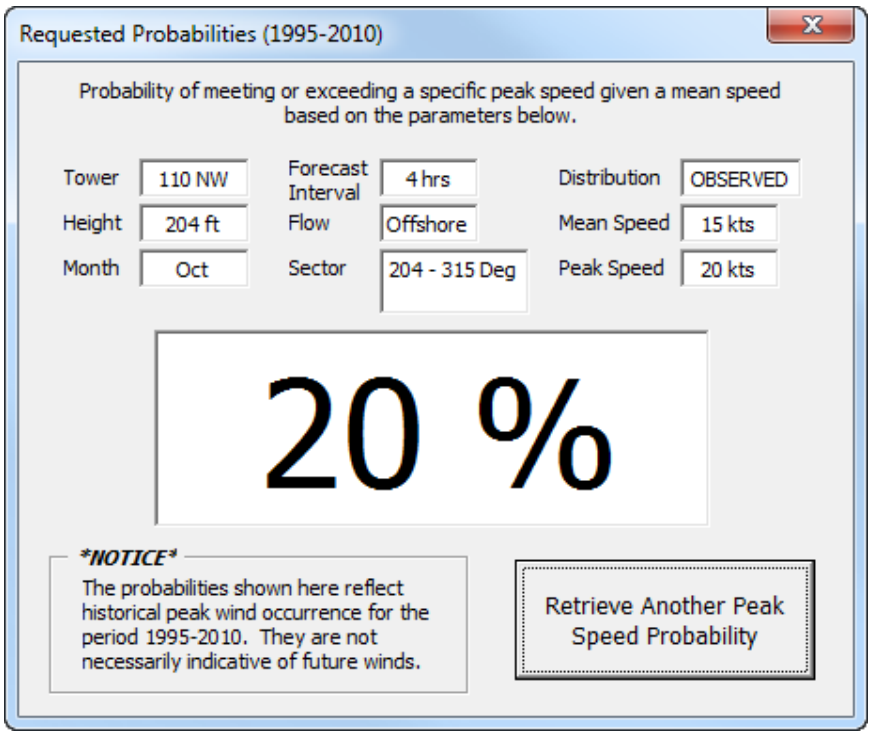

Figure 17. Output form displayed showing the probability of meeting or exceeding 20 kt over the next four hours when the mean speed is 15 kt during offshore flow at the 230-ft sensor on the northwest tower of SLC 41 in October after clicking the "Get Probability..." button in the mean and peak choice form. The format is the same for the diagnostic and prognostic probabilities.

5. Summary

Accurate forecasts of peak winds are critical to protecting the safety of launch pad workers on KSC/CCAFS and preventing financial losses due to delays and damage. However, peak winds are a challenging parameter to forecast, particularly in the cool season. To help alleviate the difficulty in forecasting peak winds, the 45 WS tasked the AMU to

- Update the Phase III peak speed statistics for the LCC towers by increasing the POR from 13 to 16 years,
- Stratify the data by onshore/offshore flow, and
- Update the Phase III GUI to display the desired values.

The AMU met the goals in this work and delivered the GUI to the 45 WS for operational use. While stability is an important factor in the magnitude of peak winds, the data were not stratified by stability due to the issues described in section 2.3.4. Users of the GUI must take this into account when interpreting the output.

5.1 Statistics

The AMU created the climatologies of the mean and peak wind speeds similar to those in Phase III. The difference is that the values represent the climatologies for every hour in an onshore or offshore regime for each tower, height, and month. It is important to note that the climatologies are smoothed values of highly variable data and are not to be used to determine the mean and peak winds for a particular time on a particular day. These values would be useful in the time leading up to an operation to show forecasters the average speeds at a particular tower and height for a particular month, hour, and/or flow regime.

After the climatologies, the AMU created the diagnostic peak speed probabilities for the 5-min mean speeds in 1-kt intervals. Diagnostic indicates that the peak speeds were associated with the mean speed from the same 5-min period. As in Phase III, the Gumbel distribution was fit to the data, except for the higher speeds. An objective two-step algorithm developed by the AMU in Phase III was used to determine the highest speed that could be modeled with the Gumbel distribution.

The final set of statistics calculated were the prognostic probabilities that provide the probability of meeting or exceeding a specified peak speed within a specified time period after a 5-min mean speed observation. The time periods requested by the 45 WS were 2, 4, 8, and 12 hours. The AMU used a re-sampling technique developed in Phase III that used all 5-min mean and peak speeds in the data set to calculate the empirical probabilities. Due to the extra time needed to modify this technique to account for the new $\geq$ 5kt/upwind filters and onshore/offshore stratifications and the requirement that work be completed by 30 September at the end of the AMU contract, the AMU was able to complete the 2- and 4-hour probabilities, but not the 8- and 12-hour probabilities.

The AMU modified the GUI developed in Phase III to accommodate the new onshore/offshore stratifications for the climatologies and probabilities. This GUI was delivered to the 45 WS during development to test and make suggestions for modifications, all of which were incorporated. This ensured that the end product met their needs, was easy to use, and produced useful information in a readable format.

5.2 Future Work

Several factors influence the intensity of peak winds on KSC/CCAFS. The phenomena responsible for high mean and peak speeds include frontal passages, convective outflow boundaries, and the mixing down of high momentum air from aloft. The atmospheric stability in the boundary layer is also an important factor for gusts, as is the location of the wind sensor relative to the ocean (i.e. how far inland), how much vegetation surrounds the site, and the placement of the sensor relative to the tower.

5.2.1 SLC 41 Towers

The issues surrounding the placement of the wind sensors on the lightning protection towers at SLC 41 are discussed in section 2.3.1.4. The simplest and lowest cost solution to solving the placement issue is to move the sensor on the southeast tower to the eastern-most point on that tower. This would ensure that winds from the east-northeast would be upwind of this sensor. The same can be accomplished by moving the sensor on the northwest tower to the northern-most point. Either solution would work, but only one should be chosen so that winds from the east-northeast will be upwind for one of the sensors.

Another issue with these sensors is the length of the boom in relation to the width of the tower. The boom on the southeast tower is shown in Figure 18 extending to the left of the tower. It appears shorter than the width of the tower. A boom that is too short would require the buffer angle from the tower sides be larger. Head winds could also cause a problem due to turbulent back-eddies from wind buffeting the tower. A boom of proper length would put the sensor beyond such a turbulent zone. The World Meteorological Organization (WMO) states that a boom length should be at least three times the width of the tower (WMO 2008) to alleviate exposure to turbulence from the tower. The WMO is not explicit about the type of tower, whether solid or lattice, and it could be that the effective width of the SLC 41 towers is smaller than the actual width. This width should be determined so the effects on the resulting wind observations can be evaluated. An optimal boom length for the width of the towers should also be determined. Depending on length, the boom may have to be supported to minimize wobble. At the very least, the effects of the current exposure should be determined so LWOs can understand the impacts on the observations they are using to evaluate the LCC.

Figure 18. The SLC 41 southeast lightning protection tower and wind sensor, looking west-northwest. The sensor and boom are highlighted by the yellow ellipse. The top of the southwest lightning tower is in the background.

5.2.2 Stability

Stability is an important factor for the magnitude of peak winds as found in several previous studies (e.g. Monahan and Armendiraz 1971, Paulsen and Schroeder 2005). The AMU calculated the stability at several towers using R_i and R_B and found these values to be < 0.25 a large percentage of the time, indicating instability even in stable regimes. Therefore, the AMU decided to attempt determining stability using the ML height from the CCAFS soundings. Due to the time needed to modify and test an existing algorithm in use by scientists in ENSCO's GS Division, the results could not be provided to the AMU in time to complete this work before the 30 September deadline. Dr. Merceret investigated the relationship of a solar parameter to gust factors as a proxy for stability. He found good fits with linear regression between the solar parameter and the gust factor means and standard deviations. However, he found the performance of the solar parameter vs. the Gumbel distribution was similar, with the Gumbel distribution performing slightly better.

The above findings resulted in the data not being stratified by stability prior to calculating the statistics. Given the known importance of this parameter, it should be used as a stratification parameter in the next follow on report. The code to create the ML heights is now complete and can be used to calculate these values from the CCAFS sounding. These values will be used in calculating the stability of the boundary layer over KSC/CCAFS.

5.2.3 Other Phenomena and Resulting Distributions

The peak speed distributions from frontal passages, convective outflow boundaries, and the mixing down of high momentum air from aloft could result in different parametric distributions. In this study, the Gumbel distribution produced a good fit to the diagnostic C-CDFs created from distributions with at least 100 observations, but not the higher speeds with fewer observations. It is important to keep in mind that the factors creating gusts at higher speeds also create gusts at the well-sampled lower speeds. It is possible that the peak speed distributions at the lower mean speeds are the sum of a mixture of multiple population samples with different distributions. The different phenomena that cause gusts could occur at the same time, and each could create their own distribution that is not necessarily Gumbel, but the sum of which is approximately Gumbel.

The best way to determine the proper distributions would be to create data stratifications based on meteorological phenomena and other physical properties such as topography around the tower as well as stability. Sounding or tower temperature data could be used to determine stability, but a complex algorithm would have to be developed to recognize the patterns and observations associated with other meteorological phenomena. Also, care must be taken not to stratify the data with too many categories to avoid creating samples too small to calculate robust statistics. One option to avoid this would be to not stratify by month or hour, but rather by the physical properties and phenomena that create peak winds. One possibility is to stratify by the cool season synoptic regimes used by 45 WS forecasters. In any case, future work on this topic should include stratification by physical processes.

5.3 Conclusions

The onshore and offshore climatologies developed by the AMU in this task will be used to assist LWOs in evaluating the peak wind thresholds for each launch vehicle. They can be used in the months and weeks ahead of a launch on the day of launch to advise launch customers of the climatology of the day and time of launch and the probability of meeting or exceeding the threshold peak speed based on a forecast mean speed. It is important to remember that all climatology and probability values calculated in this task represent historical wind behavior. They are not predictive, and should not be used as an absolute forecast of future winds. They are intended to assist in making the forecast as an objective first guess. Model output, current observations, and forecaster experience should be used along with this tool to make a confident peak wind forecast.

Appendix

Stability Calculations

Richardson Number

The AMU determined that the gradient and bulk Richardson numbers (Ri and R_B; Stull 1988) using tower and sounding data, respectively, would be used to determine the stability stratifications. The equation is similar for both:

$$\mathrm{Ri} = \frac{\frac{g}{\overline{\Theta}_v}\frac{\partial \overline{\Theta}_v}{\partial z}}{\left[\left(\frac{\partial \overline{U}}{\partial z}\right)^2 + \left(\frac{\partial \overline{V}}{\partial z}\right)^2\right]}$$

where g is gravity, z is height, Θ_v is the virtual potential temperature, and U/V are the horizontal wind components. The horizontal bar over Θ_v, U, and V indicate a time-averaged value, in this case 5 minutes. For the towers, Ri was calculated at each level. The AMU planned to calculate R_B using data from the surface and ML top levels in the soundings. The values for Table 4 were calculated from Tower 2 levels 6, 12, 54, 90, 145, and 204 ft, and Tower 313 levels 6, 12, 54, 162, 204, 295, 394, and 492 ft.

Virtual Potential Temperature

The tower data needed to calculate Θ_v are temperature (T) and dew point temperature (T_d). The first step was to calculate vapor pressure, e, using T_d (Rogers and Yau 1989):

$$e = 6.112\exp\left[\frac{17.67(T_d)}{T_d + 243.5}\right].$$

Next, the mixing ratio, w, was calculated using e and pressure (p):

$$w = \frac{0.622(e)}{p - e}.$$

The potential temperature, Θ, was calculated using Poisson's Equation:

$$\Theta = T\left(\frac{1000\mathrm{mb}}{p}\right)^{0.286}.$$

This value and w were used to calculate Θ_v:

$$\Theta_v = \Theta[1 + 0.61(w)].$$

The wind towers do not have barometers to measure pressure, so the pressure at each level of the tower had to be estimated. These pressures were calculated using a derivation of the hydrostatic equation in which the lapse rate along the tower is constant (Hess 1959):

$$p = p_0\left(\frac{T}{T_0}\right)^{\frac{g}{R\gamma}},$$

where p is the pressure at a tower level, p_0 is the surface pressure, T is the tower level temperature, T_0 is the surface temperature, g is gravity, R is the gas constant for dry air, and γ is the lapse rate. The hourly SLF sea level pressure was used for p_0 and the 6-ft temperature was T_0.

Wind Components

The wind data are provided as speed in knots and direction in degrees. Ms. Crawford converted these values to u and v components using

$$u = spd \times \cos\left[(270 - dir) \times \frac{\pi}{180}\right] \text{ and}$$

$$v = spd \times \sin\left[(270 - dir) \times \frac{\pi}{180}\right],$$

where spd is the speed in m/s and dir is the direction in degrees. Ms. Crawford converted the speed from knots to m/s with the relation

$$spd = speed(kt) \times 0.5175.$$

Solar Parameter

Background

The solar parameter (S) discussed in section 2.3.4.3 and plotted in Figure 5 is the sine of the angle of elevation of the sun above the horizon. It is a direct geometrical measure of the ratio of the incident solar radiation per unit area of the earth's surface to the radiation received on an equal area of surface normal to the incoming solar radiation. At the top of the atmosphere, a surface normal to the incoming sunlight receives approximately 1365 Wm^{-2} of incident solar radiation, which is known as the solar constant (I_s). Globally, on average, about 30% of this is scattered, reflected or absorbed by the atmosphere before it can reach the surface of the earth. Thus, in the absence of overcast, fog, haze or similar phenomena, the incident energy per unit area at the earth's surface, I_e, is roughly given by

$$I_e = 0.7 * I_s * S.$$

Use of a measure of solar intensity was explored for this project because it is well known that gust factors (i.e. peak winds at a given mean wind speed) depend on atmospheric stability. Dr. Merceret found that traditional stability measures calculated from measured vertical temperature and wind profiles did not appear well correlated with the gust factors in this task's data. In central Florida, typically stable conditions occur at night with radiative surface cooling and unstable conditions occur in the daytime when the sun heats the surface. The correlations are not perfect and there are many additional contributors to stability in a given environment beyond the intensity of incoming radiation. Nonetheless, solar intensity was a variable with two strong advantages:

- There is a physical basis for considering it as one among several predictors for the gust factor, and
- It is easy to calculate unambiguously and precisely.

Since there are no sensors within the tower network to measure the actual solar intensity on an hourly basis, S was selected as the measure of solar intensity. In reality, the actual solar intensity is $\leq I_e$ depending on the extent to which overcast, fog, haze or similar phenomena are present. Since $0.7 * I_s$ is constant and amounts only to a scale factor, Dr. Merceret used S rather than I_e as the predictor. He expected that with the large sample size, the effects of cloudiness would result in some scatter in the data, but not enough to mask useful relationships that might be present.

Linear Regression

Initial examination of the suitability of S as a predictor for the gust factor (GF) consisted of plots of S and GF as a function of time such in Figure 5 of section 2.3.4.3. Those strongly suggested that both the mean and variance of the GF were correlated with S. To quantify this correlation, regressions were

performed using S as the independent variable and either the mean or the standard deviation of the GF as the dependent variable. The regressions corresponding to Figure 5 in the report are in Figure 19. The regressions for the mean GF accounted for more than 95% of the variance. The regressions for the standard deviations were not as good, but still accounted for more than 70% of the variance in the standard deviation.

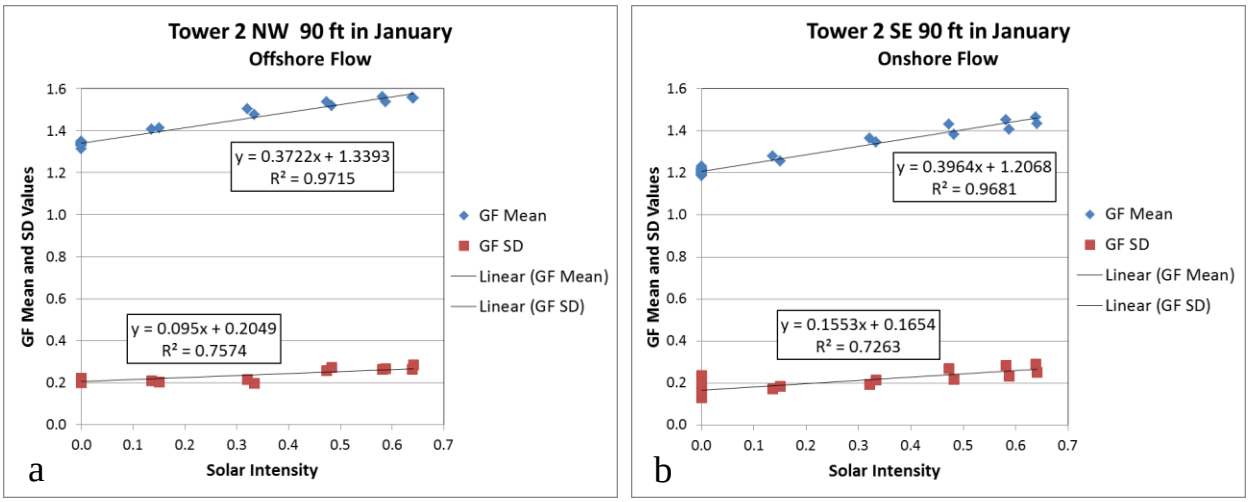

Figure 19. Linear regression of the GF mean and standard deviation vs solar parameter in January for a) offshore flow on the northwest side of Tower 2 at 90 ft, and b) onshore flow on the southeast side of Tower 2 at 90 ft.

The solar parameter proved to be an extremely useful, physics-based predictor for the statistical properties of the GF, but it has two obvious weaknesses:

1) It cannot account for any variation of the GF between sunset and sunrise, and
2) It cannot take into account variations in GF due to reductions in I_e due to cloudiness.

Comparison to Gumbel Distribution

Although not physics-based, the purely empirical Gumbel distribution should capture the statistical influences of these things on the probability distribution of the GF. Unfortunately, there was not sufficient time or resources in the project to incorporate both methodologies into the final product. In order to select which one to use, Dr. Merceret compared the predicted probability distributions with the observed distributions in a reliability diagram for the samples used to generate the solar and Gumbel regressions. Although these were not independent samples, they could illuminate the details of how each technique allocated the samples within the range of values in the distribution. Since the solar parameter was expected to be ineffective during the dusk-night-dawn period, data in this period (2200-1300 UTC, 1700-0800 EST, roughly 1720-0820 local solar time) were combined into one stratification. The solar parameter should show its strongest effects near solar noon, so a mid-day stratification was created covering 1600-1900 UTC (1100-1400 EST, 1120-1420 local solar time). All remaining hours of the day were combined in a morning-afternoon stratification. This was done for Tower 2 at 54 ft in January only since time constraints required a decision be made without further delay. One complication was that the Gumbel distributions were generated based on a stratification by mean wind speed while the solar parameter was applied independent of wind speed. Therefore, the comparisons had to be stratified by both time of day and wind speed. This reduced the sample size markedly at higher wind speeds.

The reliability diagram in Figure 20 is typical of the dusk-night-dawn stratification at moderate wind speeds. As expected, the Gumbel model worked well and the solar model less so. This was true at all wind speeds for this stratification, although the solar and the Gumbel probabilities differed by less than 10% at the lowest wind speeds.

Figure 21a shows that when the sun is well above the horizon, the solar parameter does better than the Gumbel at lower wind speeds, again as expected. At higher wind speeds, the Gumbel appears to do better even during the mid-day as shown in Figure 21b. One possible explanation for this is that the higher wind speeds may be associated with winter storms and frontal passages that are accompanied by substantial cloudiness. This invalidates the use of S in place of the actual, cloud-influenced I_e as the predictor. There was not time to attempt to validate this hypothesis, but if it is correct, the acquisition and application of a solar irradiance sensor might improve the predictability of peak winds in the area.

The morning-afternoon results (not shown) were similar to those for mid-day. Based on these figures, the tool will contain probabilities based on the Gumbel distribution. It is likely that a significantly better tool could be developed if multiple, physics-based factors could be considered simultaneously. These would include wind speed, solar intensity (preferably actual measured values) and synoptic situation.

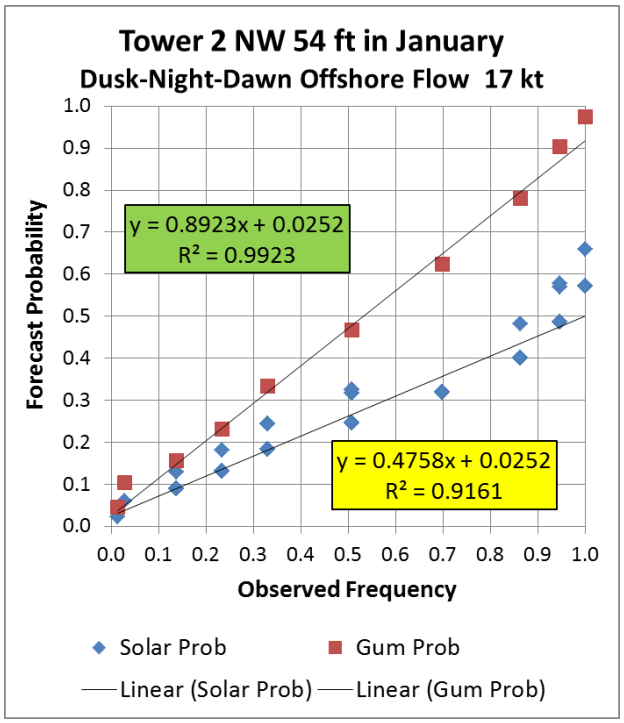

Figure 20. Reliability diagram for Tower 2 at 54 ft in January for an offshore mean wind speed of 17 kt with the sun below the horizon. The solar regression is in the box with the yellow background, the Gumbel regression is in the box with the green background. A perfect model would have a slope of 1, an intercept of 0 and $R^2 = 1$.

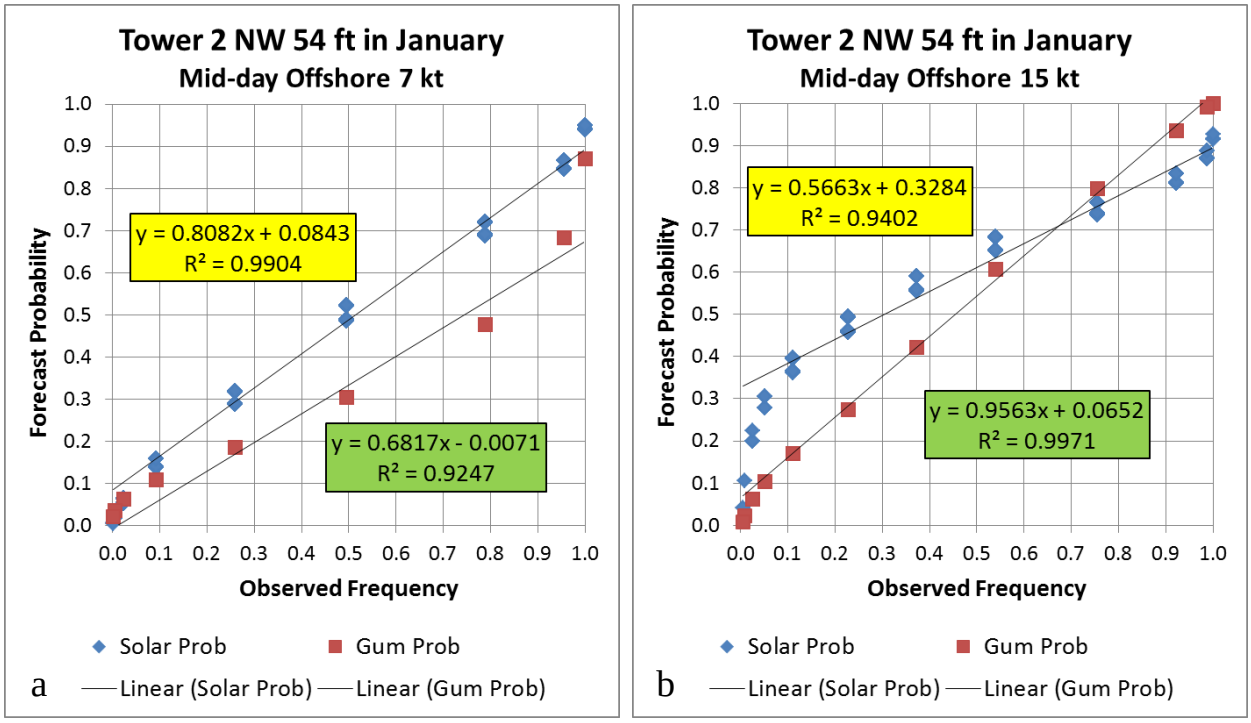

Figure 21. Same as Figure 20 except for during mid-day and a) 7-kt mean speed and b) 15-kt mean speed.

List of Acronyms

45 WS	45th Weather Squadron
AMU	Applied Meteorology Unit
CCAFS	Cape Canaveral Air Force Station
CDF	Cumulative Distribution Function
C-CDF	Complementary CDF
GF	Gust Factor
GUI	Graphical User Interface
GS	GeoSystem Solutions, an ENSCO division
KSC	Kennedy Space Center
LCC	Launch Commit Criteria
LWO	Launch Weather Officer
ML	Mixed Layer
PDF	Probability Density Function
POR	Period of Record
QC	Quality Control
S	Solar Parameter
SLC	Space Launch Complex
SLF	Shuttle Landing Facility
VBA	Visual Basic for Applications (Excel)
WMO	World Meteorological Organization

References

Barrett, J. H., 2010: Peak Wind Tool for General Forecasting Phase II. NASA Contractor Report CR-2010-216289, Kennedy Space Center, FL, 57 pp. [Available from ENSCO, Inc., 1980 N. Atlantic Ave., Suite 830, Cocoa Beach, FL, 32931 and online at http://science.ksc.nasa.gov/amu/final.html.]

Bauman, W. H. III, 2010: Verify MesoNAM Performance. NASA Contractor Report CR-2010-216287, Kennedy Space Center, FL, 31 pp. [Available from ENSCO, Inc., 1980 N. Atlantic Ave., Suite 830, Cocoa Beach, 32931, and at http://science.ksc.nasa.gov/amu/final.html.]

Crawford, W. C., 2010: Statistical Short-Range Guidance for Peak Wind Forecasts on Kennedy Space Center/Cape Canaveral Air Force Station, Phase III. NASA Contractor Report CR-2010-216281, Kennedy Space Center, FL, 33 pp. [Available from ENSCO, Inc., 1980 N. Atlantic Ave., Suite 830, Cocoa Beach, FL, 32931 and online at http://science.ksc.nasa.gov/amu/final.html.]

Hess, S. L., 1959: *Introduction to Theoretical Meteorology*. Robert E. Krieger Publishing Company, Malabar, FL, 364 pp.

Lambert, W. C., 2002: Statistical short-range guidance for peak wind speed forecasts on Kennedy Space Center/Cape Canaveral Air Force Station: Phase I Results. NASA Contractor Report CR-2002-211180, Kennedy Space Center, FL, 39 pp. [Available from ENSCO, Inc., 1980 N. Atlantic Ave., Suite 830, Cocoa Beach, FL, 32931 and online at http://science.ksc.nasa.gov/amu/final.html.]

Lambert, W. C., 2003: Extended Statistical Short-Range Guidance for Peak Wind Speed Analyses at the Shuttle Landing Facility: Phase II Results. NASA Contractor Report CR-2003-211188, Kennedy Space Center, FL, 27 pp. [Available from ENSCO, Inc., 1980 N. Atlantic Ave., Suite 830, Cocoa Beach, FL, 32931 and online at http://science.ksc.nasa.gov/amu/final.html.]

Monahan, H.H. and M. Armendariz (1971): Gust Factor Variations with Height and Atmospheric Stability, J. Geophys. Res., **76**, 5807 - 5818

Paulsen, B. M. and J. L. Schroeder, 2005: An Examination of Tropical and Extratropical Gust Factors and the Associated Wind Speed Histograms, J. Appl. Meteor., **44**, 270 -280.

Rogers, R. R. and M. K. Yau, 1989: *A Short Course in Cloud Physics*. Pergamon Press, New York, NY, 293 pp.

Stull, R. B, 1988: *An Introduction to Boundary Layer Meteorology*. Kluwer Academic Publishers, Dordrecht, The Netherlands, 670 pp.

Wilks, D. S., 2006: *Statistical Methods in the Atmospheric Sciences*. 2d ed. Academic Press, Inc., San Diego, CA, 467 pp.

World Meteorological Organization, 2008: Guide to Meteorological Instruments and Methods of Observation, WMO-No. 8, Seventh Edition. [Available online at http://www.wmo.int/pages/prog/www/IMOP/publications/CIMO-Guide/CIMO_Guide-7th_Edition-2008.html.]

NOTICE

Mention of a copyrighted, trademarked or proprietary product, service, or document does not constitute endorsement thereof by the author, ENSCO Inc., the AMU, the National Aeronautics and Space Administration, or the United States Government. Any such mention is solely for the purpose of fully informing the reader of the resources used to conduct the work reported herein.